J. Fluid Mech. (1986), *vol.* 167, *pp.* 49–64
Printed in Great Britain

Onset of surface-tension-driven Bénard convection

By E. L. KOSCHMIEDER AND M. I. BIGGERSTAFF
College of Engineering and I. Prigogine Center for Statistical Mechanics,
The University of Texas, Austin, TX 78712, USA

(Received 4 April 1985 and in revised form 20 November 1985)

An experimental investigation of the onset of convection in shallow fluid layers heated uniformly from below and cooled from above by an air layer has been made. If the depth of the silicone layer is smaller than 2 mm the onset of convection takes place in two stages. There is first a weak pattern, which is characterized by its appearance at ever smaller temperature gradients as the depth of the fluid is decreased. When the temperature difference across the fluid is increased a second strong pattern forms near the predicted critical Marangoni number. The cells in this pattern are hexagonal and seem to be what one has always referred to as Bénard cells. The temperature gradient at which this pattern appears increases with decreased depth. The heat transfer through the fluid has been measured. The critical temperature gradient for the formation of the hexagonal pattern has been determined from the break of the heat transfer curve.

1. Introduction

The investigations of Bénard (1900) marked the beginning of the study of fluid motions in a shallow fluid layer heated uniformly from below. The most notable observation of Bénard was the hexagonal convection cells, now commonly referred to as Bénard cells. Today, 86 years later, we still do not possess a convincing explanation for the formation of the hexagonal cells, and for the preference for hexagonal cells over the other possible cellular patterns.

Rayleigh's (1916) pioneering theoretical analysis of the stability of a layer of fluid heated from below seemed to provide a basis for the understanding of the Bénard cells. Rayleigh's most fundamental result however was the discovery of the existence of a critical or minimal temperature gradient required for the onset of convection. Bénard had not noticed the existence of such a critical gradient in his experiments. Actually, in a later evaluation of his experiments (Bénard 1930), he came to the conclusion that he had observed convection at temperature differences about 10^{-4} to 10^{-5} times smaller than the critical temperature gradient predicted by Rayleigh. Bénard's interpretation of his own experiments was ignored. We shall see in the following that his interpretation of his experiments was correct.

A new aspect was introduced into the explanation of the Bénard cells by Block (1956). He concluded from his experiments that surface tension must play a significant role in the formation of the hexagonal cells. He also pointed out that convective motions occurred at temperature differences of a fraction of the predicted critical value. A short time thereafter the same points were established theoretically by Pearson (1958). Pearson, who investigated surface forces only, showed that the onset of surface-tension-driven convection is determined by the critical value of a non-dimensional parameter, the Marangoni number. From the value of the critical

Marangoni number, and from the linear dependence of the Marangoni number on the depth of the fluid it follows that the onset of convection in shallow fluid layers should occur at critical temperature differences much smaller than those predicted by Rayleigh's theory. An explanation for the discrepancies of the experimental and theoretical values of the critical temperature difference had apparently been found. However, we will show in the following that the onset of surface-tension-driven convection occurs at temperature differences significantly below those predicted by the critical Marangoni number.

Pearson's theory has been augmented by the studies of Nield (1964), and Scriven & Sternling (1964). Nield studied the conditions for the onset of surface-tension-driven convection in the presence of gravity, i.e. he dealt with the situation experienced in the laboratory and obviously present in Bénard's experiments. He found that surface-tension-driven convection and buoyancy-driven convection are coupled. In the case of very shallow fluid layers the minimal temperature difference required for the onset of convection in the presence of gravity is, according to Nield, determined by the critical Marangoni number. Scriven & Sternling neglect gravity, just as Pearson did, but take various other parameters into account, in particular the surface tension coefficient S, not only the variation of surface tension with temperature $\mathrm{d}S/\mathrm{d}T$, in which form surface tension appears in the Marangoni number. Smith (1966) extended these two studies by considering the effect of gravity waves. He found that surface waves are usually important only for very small wavenumbers.

The results of Scriven & Sternling differ drastically from those of Pearson as well as Nield. They find that onset of convection in very shallow fluid layers can occur at very small temperature differences, the onset temperature difference decreasing with decreased fluid depth. This differs clearly from the result to be expected when either the critical Marangoni number or the critical Rayleigh number determine the onset of motion. An onset of convection governed by, for example, the critical Marangoni number implies that the critical temperature gradient increases as the depth of the fluid is decreased. As will be shown in the following, the onset of convection with a free (air) surface actually occurs at smaller temperature differences if the fluid depth is decreased, provided that the depth of the fluid is smaller than a certain value above which the conventional critical Marangoni number determines the onset of motion.

The stability of a non-deformable fluid layer subject to buoyancy and surface-tension forces has been investigated with the energy method by Davis (1969). Davis finds a subcritical instability in a small range of Marangoni numbers for sufficiently small Rayleigh numbers. These energy method studies have been confirmed by Davis & Homsy (1980) with an investigation of the same problem but with a deformable surface. Castillo & Velarde (1982) have studied, also with the energy method, the stability of two-component or one-component fluid layers with a deformable surface heated from below or from above, and found likewise this subcritical instability.

Nonlinear theoretical studies of surface-tension-driven convection have been made by Scanlon & Segel (1967), Kraska & Sani (1979), and Cloot & Lebon (1984), all trying to explain the preference for the hexagonal cells. Recently Rosenblat, Davis & Homsy (1982*a*, *b*) have investigated surface-tension-driven convection in bounded circular or rectangular fluid layers of small aspect ratio. There are only two modern experimental investigations of surface-tension-driven Bénard convection. Koschmieder (1967) observed the formation of a regular hexagonal cell pattern and determined the wavelength of the convective motions. Palmer & Berg (1971) determined the critical Marangoni number from the break of the heat transfer curve which is caused

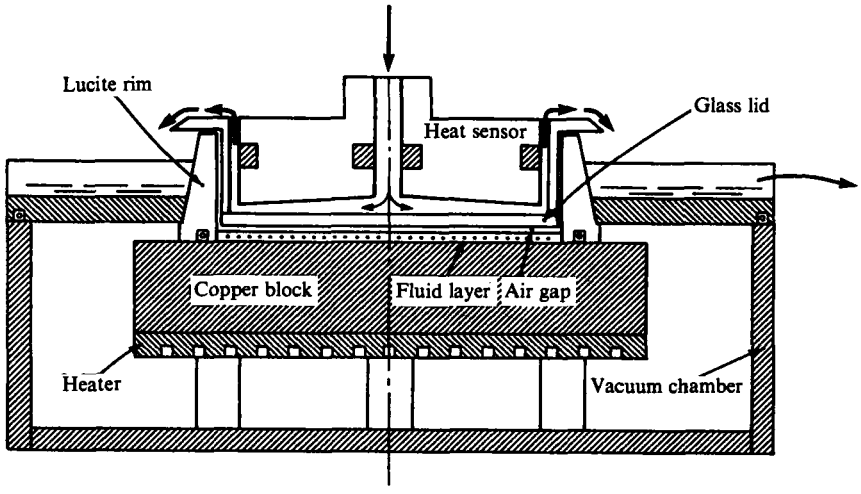

FIGURE 1. Schematic section though the convection apparatus.

by the onset of the convective motions. These two sets of experiments were made with fluid layers 2–5 mm deep. We will show in the following that one has to go to layers less than 2 mm deep in order to observe purely surface-tension-driven motions. Bénard's experiments were made with fluid layers of depths ranging from about 1 mm to about 0.5 mm.

2. Description of the apparatus

The apparatus used is a modified version of an apparatus used previously by Koschmieder & Pallas (1974*a*). A schematic diagram of the apparatus is shown in figure 1. The bottom of the fluid layer was a 5 cm thick copper block, which was heated from below by an electric current going through a resistance wire. The wire was cemented in circular grooves in a brass plate. The excellent thermal conductivity and the thickness of the copper block in combination with poor thermal conduction on top assure that the temperature at the top of the copper plate is practically uniform, as is required for comparison with the theories describing Bénard convection. To avoid lateral heat losses the copper block was placed in a vacuum tank. The copper plate was covered by shallow layers of silicone oil, bounded laterally by a circular lucite rim of 13.55 cm diameter. With a fluid depth of say 1 mm the aspect ratio of the fluid, defined as the ratio of the horizontal extension of the fluid divided by the fluid depth, was 135. The fluid was cooled from above through a very thin layer of air between 0.3 and 0.5 mm deep. The air was bounded on top by a glass plate 2.3 mm thick. The glass plate was the bottom of a lid in which water was circulated at a rate of 80 $cm^3\ s^{-1}$ in order to fix the temperature of the glass plate and thereby the temperature on top of the fluid.

Most of the space above the glass plate was filled usually with the so-called heat sensor, a device to measure the increase of the temperature of the cooling water caused by the heat transferred through the fluid layer and the air above it. The heat sensor is essentially a thermopile of 10 thermocouples in series, measuring the temperature difference between a copper ring surrounding the water inlet and copper ring being in contact with the cooling water after it passed over the glass plate.The heat sensor

has been described in detail elsewhere (Koschmieder & Pallas 1974*b*). Temperature differences of 0.001 °C between the incoming and outgoing water can be measured with the heat sensor. From the measured temperature increase of the cooling water follows the heat flux through the fluid layer, as will be discussed later.

The cooling water was taken from a 50 l insulated tank filled with water. The temperature of the water in the insulated tank was controlled by a heat exchanger whose temperature was determined by water coming from a commercial regulated water bath. Cooling water cannot be used from the water bath directly as the heat sensor is too sensitive. The heat sensor picks up the fairly regular fluctuations of the water temperature of the bath, which are caused by the heating and cooling of the temperature control. The enormous heat capacity of the water in the insulated tank reduces the fluctuations of the water-bath temperature. A steady signal for the temperature difference between incoming and outgoing water was then obtained.

3. The experiments

3.1. *Pattern formation*

The fluid motions were made visible by aluminum powder suspended in the fluid, which was either 100 cs silicone oil, or in some cases 50 cs silicone oil (Dow Corning 200 fluid). The properties of both fluids are listed in table 1. All experiments were made in a nearly steady state, it took usually about eight hours to heat up the fluid from rest at zero temperature difference to the highest temperature difference applied, which was in the maximal case about 60 °C between the copper plate and the glass lid. The fluid depth in the experiment shown in figure 2 was 1.37 mm, the depth of the air gap on top of the fluid was 0.5 mm.

When the fluid layer is heated up the first faint sign of motion is, besides a strong roll along the rim, a system of circular concentric rings, see figure 2(*a*). There are, in this picture, two stronger individual cells, which are caused by two impurities which have come into the fluid with the aluminum powder. The convecting fluid is seen on the shiny copper plate through the lid covering the fluid layer. The lid is filled with cooling water in order to maintain the temperature difference across the fluid. The heat sensor is taken out of the lid. Increasing the temperature difference causes the rings in figure 2(*a*) to break up into cells, figure 2(*b*). The cells clearly have a centre, the cell outline on the other hand is rather weak and not regular, certainly not of a regular hexagonal form. Increasing ΔT further intensifies the cells, figure 2(*c*). The cell boundaries then become outlined by floating aluminum powder which is extruded from the fluid. In figure 2 a larger than usual amount of aluminum powder was added to the fluid in order to be able to see the flow on photographs. In figure 2(*c*) the extruded aluminum powder can be seen floating on the surface of the fluid in the space between the outermost ring of cells and the clearly visible rim roll.

When the temperature difference is increased further a very definite change in appearance of the cells occurs spontaneously at a certain reproducible (critical) temperature difference ΔT_2, as can be recognized clearly in figure 2(*d*). The new type of cell is strikingly reminiscent of Bénard cells as we have seen them many times before, a good example of such a pattern can be found in Koschmieder (1974). As the hexagonal cells form, the floating aluminum powder, which outlined the cells of the first pattern, disappears from the surface of the fluid. Some aluminum powder then settles at the bottom in the centre of the cells underneath the uprising fluid. The settled powder can be recognized as little black specks in figure 2(*d*). The appearance of the hexagonal cells is also accompanied by an increase of the heat flux

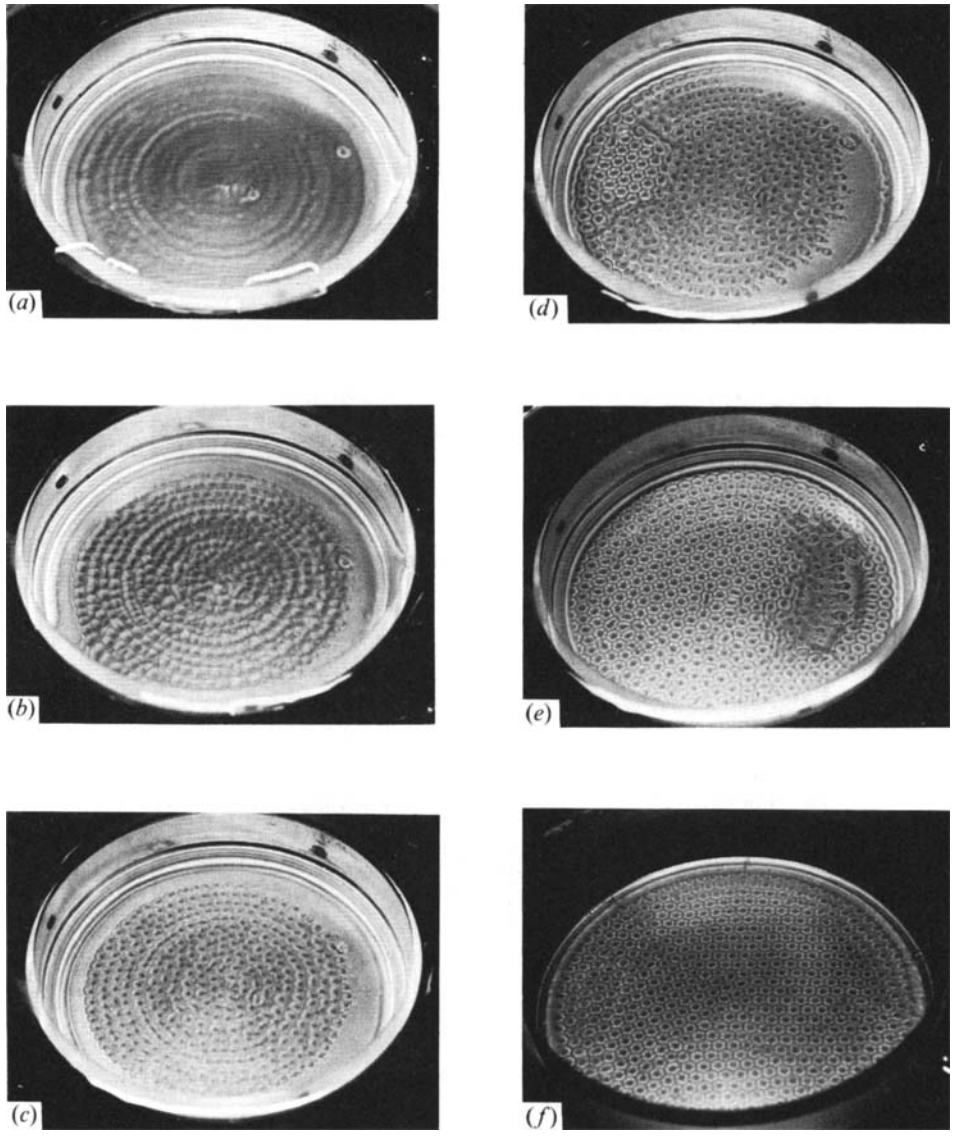

FIGURE 2. Visualization of the onset of convection in a layer of silicone oil of 100 cs viscosity, 1.37 mm deep, with an air gap of 0.51 mm. (*a*) $\Delta T = 0.57\ \Delta T_2$; (*b*) $0.72\ \Delta T_2$; (*c*) $0.86\ \Delta T_2$; (*d*) $0.95\ \Delta T_2$; (*e*) ΔT_2; (*f*) $1.08\ \Delta T_2$.

through the fluid layer, as will be shown later. A truly critical transition should, under ideal conditions, occur simultaneously over the entire area of the fluid. We have not observed such a genuine transition because of experimental difficulties. In particular, we cannot keep the depth of the air layer uniform over the entire area of the fluid layer. The reason for this is that the glass plate of the lid has to be glued to the frame of the lid. We have not been able to do this with an accuracy better than (at best) $\pm\frac{1}{100}$ mm. But $\frac{1}{100}$ mm is a substantial fraction of the gap between the fluid and the glass, which ranges from 0.3 to 0.5 mm in different experiments. A large portion, in many cases actually the larger part, of the applied temperature difference between

ν (cm^2/s)	ρ (g/cm^3)	α ($°C^{-1}$)	κ (cm^2/s)	S (dyne/cm)	dS/dT (dyne/cm °C)
1.00	0.968	0.00096	0.001095	19.36	−0.050
0.50	0.960	0.00104	0.001025	18.35	−0.047

TABLE 1. Properties of the fluids at 25 °C

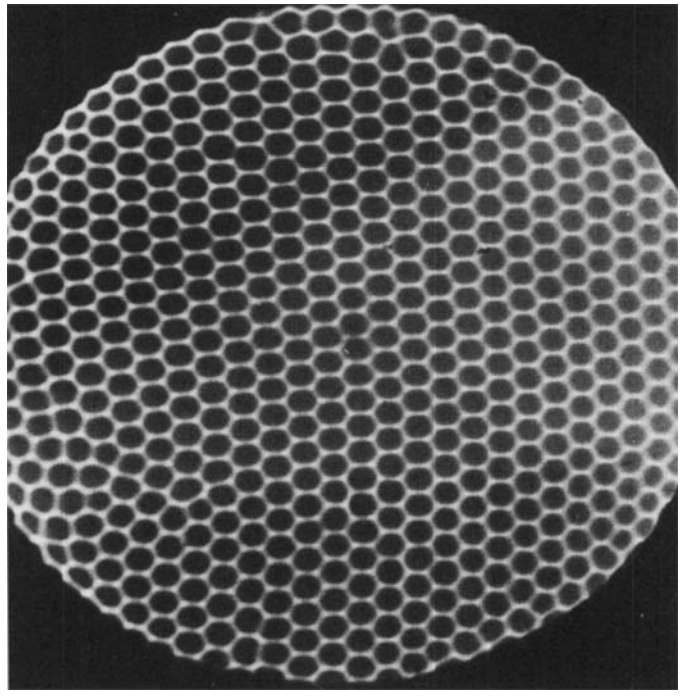

FIGURE 3. Shadowgraph of the hexagonal pattern at $\Delta T = 1.19\ \Delta T_2$. Viscosity 100 cs, fluid depth 1.35 mm.

the copper and the glass lid falls off in the air gap because of the very poor thermal conductivity of air. An air gap of unequal depth therefore causes a one-sided temperature distribution on top of the fluid. Hence the onset of the transition is one-sided.

When the temperature difference is increased further the hexagonal cells spread over an increasing area of the fluid, see figure 2 (*e*). Finally figure 2 (*f*) shows hexagonal cells covering the entire surface of the fluid. In this photograph the lid has been removed, so that one can see the rim of the layer with the rim roll, which was obscured in figure 2 (*a–e*). There are about 200 regular hexagonal cells in the pattern in figure 2 (*f*). When the slightly supercritical temperature difference is maintained another strange twist in the behaviour of the aluminum powder occurs. The small heaps of settled aluminum powder underneath the cell centres disappear, which means that the powder goes back into solution. This has never happened before in our experiments with deeper fluid layers. The peculiar behaviour of the aluminum powder does not seem to have fluid dynamics significance, but is an indication that surface forces play a role in the experiments with very shallow layers.

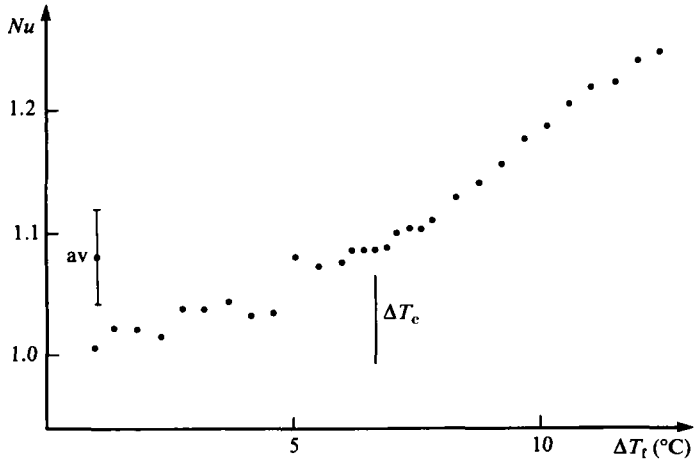

FIGURE 4. Heat transfer in the 1.81 mm deep fluid layer of 100 cs viscosity.

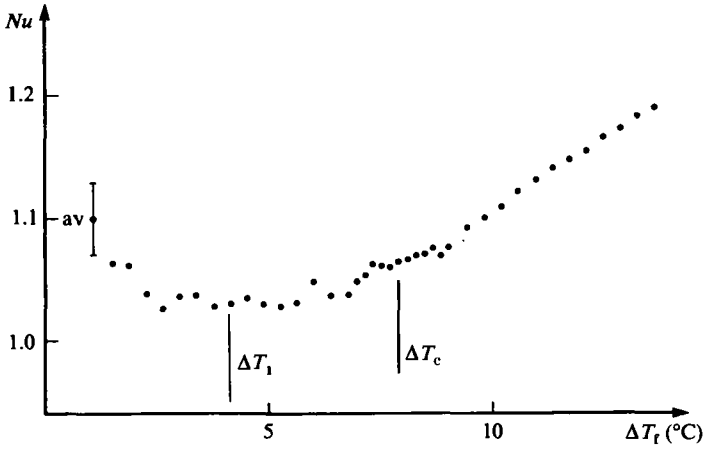

FIGURE 5. Heat transfer in the 1.31 mm deep fluid layer of 100 cs viscosity.

There is another way to visualize the fluid motions, namely the shadowgraph technique described by Silveston (1958). A parallel beam of white light is shone through the fluid layer where it is reflected from the bottom. The index of refraction in the fluid varies with temperature and consequently varies locally in the fluid with the temperature in the convective cells. The optical path of the light in the fluid layer is therefore different in different parts of a cell. Interference occurs therefore in the reflected light beam, outlining the cell pattern. We were not able to obtain a shadowgraph from the first pattern when the applied temperature difference was substantially below ΔT_2, regardless of whether we used the copper plate or a glass mirror placed on the copper plate as the bottom of the fluid. The surface of the copper block produces a shadowgraph of the second, hexagonal pattern, with minor imperfections resulting from the remaining uneveness of the copper surface caused by the machining. Shadowgraphs of the hexagonal cells obtained with the mirror were nearly perfect, see figure 3. One has to keep in mind that the mirror changes the thermal boundary condition at the bottom of the fluid, replacing the excellent

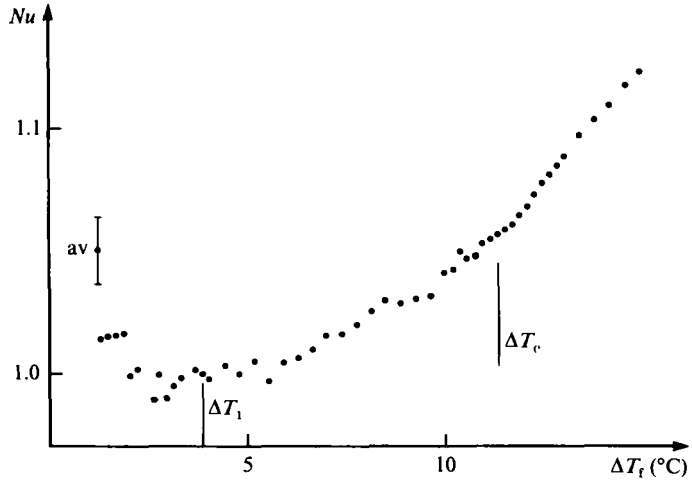

FIGURE 6. Heat transfer in the 0.93 mm deep fluid layer of 100 cs viscosity.

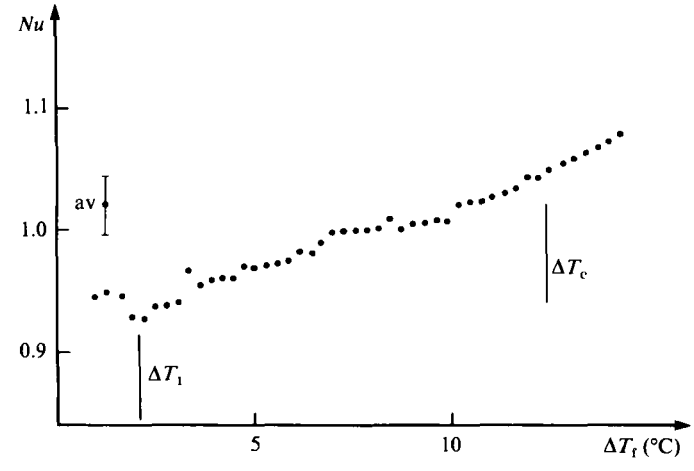

FIGURE 7. Heat transfer in the 0.72 mm deep fluid layer of 100 cs viscosity.

thermal conductivity of copper by the poor thermal conductivity of glass. The convective flow visualized by shadowgraphs with either the copper bottom or the mirror was nevertheless the same as the flow visualized with the aluminum powder.

3.2. *Heat flux measurements*

The usual procedure to determine the critical temperature gradient for the onset of convection is via the break of the heat transfer curve brought about by the additional heat transfer of the convective motions, a method introduced by Schmidt & Milverton (1935). The results of our heat transfer measurements are shown in figure 4–7. The heat flux when plotted in absolute units, or, for example, as microvolts measured by the heat sensor, has such a small change of slope with the onset of convection that the critical temperature difference cannot be determined accurately from the break of the curve. The heat flux in figures 4–7 is therefore plotted in units of the Nusselt number, which is the ratio of the actual heat flux divided by the heat flux caused

by the thermal conductivity of the fluid only. On a plot of Nusselt number versus applied temperature difference the break of the heat transfer curve is much more easily recognizable. The value of the Nusselt number before onset of convection is 1.

The abscissa in figures 4–7 is the temperature difference ΔT_f applied to the fluid. This temperature difference cannot be measured directly, because there is no space in the air gap above the fluid layer to mount thermocouples. The value of ΔT_f has to be calculated from the temperature difference ΔT between the copper plate and the cooling water. For the heat flux measurements we did not use the glass plate on top of the air layer, but a copper plate of 2 mm thickness. This was done to avoid additional corrections for the temperature drop in the glass. The value of ΔT_f is given by

$$\Delta T_f = \frac{\Delta T}{\left(1 + \frac{\bar{\lambda}_f \Delta Z_a}{\bar{\lambda}_a \Delta Z_f}\right)}, \tag{1}$$

where $\bar{\lambda}_f$ is the mean thermal conductivity in the fluid layer, $\bar{\lambda}_a$ the mean thermal conductivity in the air layer, ΔZ_a the depth of the air layer and ΔZ_f the depth of the fluid layer. ΔT can be measured with an accuracy better than 1 %. Both thermal conductivities are known only with about 1 % accuracy. The depth of the fluid is known to about 1 %, while the depth of the air layer, which is of order 0.5 mm or less, is known at best with only 2 % accuracy. So the cumulative uncertainty in the value of ΔT_f is at least 5 %. Since the Nusselt number is proportional to ΔT_f, the experimental values of Nu can differ from 1 by ± 5 % or more. It is likely that the uncertainty in the value of Nu will increase with decreased ΔZ_a and ΔZ_f, because in particular the uncertainty in ΔZ_a becomes increasingly large. All measurements of Nu give the mean value of the heat flux at a given ΔT_f determined by four experiments. The standard deviation of the four measurements determines the experimental error of the heat flux measurement. Since so many error bars would confuse the graphs, only the average value of the error bars is indicated in the figures.

We will discuss the heat flux curve of the fluid layer with 1.81 mm depth (figure 4) first. In this case it appeared from corresponding visual observations that at $\Delta T_f \approx 6.6$ °C a hexagonal pattern had established without a prior first pattern. There is, of course, an uncertainty in the visual determination of ΔT_2, because the pattern does not form spontaneously over the entire fluid. This uncertainty is of the order of 5 % of ΔT_2. As can be seen in figure 4 the heat flux is, within the experimental error, about $Nu = 1.03$ for ΔT_f up to 5 °C, then it seems to increase prior to the observed $\Delta T_2 = 6.68$ °C, and increases steadily after ΔT_2. As we will see in the data evaluation it appears that with this fluid depth the formation of the first pattern has just taken place prior to the formation of the hexagonal cells. This is also indicated by the increase in the measured Nu before ΔT_2. The increase of Nu after ΔT_2 is in agreement with expectations.

With a fluid layer of 1.31 mm (figure 5) we observed visually the formation of the first pattern at $\Delta T_1 \approx 3.7$ °C. Our heat flux measurements indicate an increase of the Nusselt number for values of $\Delta T_f < 3.7$ °C. This is caused by an erroneous signal of the heat sensor. At very small values of ΔT_f the heat flux through the fluid layer is very small. The temperature increase in the coolant measured by the heat sensor is then determined mainly by heat generated by dissipation in the cooling fluid, as it moves from the inlet over the lid to the outlet. The contribution of dissipation to the heat sensor signal decreases as the heat flux to the lid from underneath increases.

In order to obtain a signal from the heat sensor which is less affected by dissipation in the coolant, we have, in all heat flux measurements, reduced the flow rate of the cooling water to 20 $cm^3\ s^{-1}$. For values of ΔT_f between ΔT_1 and ΔT_2 at ≈ 7.9 °C the heat flux in figure 5 increases on average just a little, then increases steadily and at a faster rate after ΔT_2. There is, of course, no abrupt change in the slope of the heat transfer curve at ΔT_2 because we are dealing here with the gradual transformation of a pattern, as shown in figure 2 (*d–e*).

Figure 6 shows the heat flux for a fluid layer of 0.93 mm depth, and figure 7 for a depth of 0.72 mm. It can be seen on these figures that the critical temperature difference ΔT_2 for the formation of the hexagonal cells increases with decreased depth, while on the other hand the temperature difference ΔT_1 for the formation of the first pattern decreases with decreased depth. The values of these temperature differences for the different fluid layers are listed later in table 2. It is already apparent in figure 6 and seems to be certain in figure 7 that the heat flux through the fluid layer is no longer constant after the formation of the first pattern, but increases with increased ΔT_f. This means that the motions in the cells of the first pattern are sufficiently fast to transfer an additional amount of heat. The formation of the hexagonal cells is still marked by a clear break in the heat flux curve in figure 6, at the temperature difference at which we visually observed the transition. In figure 7 however the break in the heat flux curve is barely recognizable. This probably means that near ΔT_2 the motions in the first pattern have become so vigorous that they hardly differ from the velocity of the flow in the hexagonal cells.

We have also measured the heat flux for two fluid layers of 50 cs silicone oil. Since there is no additional significant feature in these measurements their curves will not be shown.

3.3. *Data evaluation*

In order to understand the meaning of our observations the various experimental data have to be expressed in terms of the non-dimensional parameters involved. Buoyancy driven convection is governed by the Rayleigh number, which is

$$R = \frac{\alpha g \Delta T d^3}{\nu \kappa}, \tag{2}$$

with the volume expansion coefficient α, the acceleration of gravity g, the depth of the fluid d, the kinematic viscosity ν and the thermal diffusivity κ. The critical Rayleigh number R_c for onset of convection in a fluid layer with a free surface is $R_c = 1100.6$. This value of R_c applies when the top free surface is an excellent thermal conductor. Air on top of the fluid however approximates an insulating top boundary. The critical Rayleigh number in this case is then $R_c = 669$ (Nield 1964).

Surface-tension-driven convection is governed by the Marangoni number, which is

$$Ma = \frac{\mathrm{d}S}{\mathrm{d}T} \frac{\Delta T d}{\rho \nu \kappa}, \tag{3}$$

where $\mathrm{d}S/\mathrm{d}T$ is the variation of the surface-tension coefficient with temperature, d is again the depth of the fluid, and ρ is the density of the fluid. The critical Marangoni number Ma_c with an insulating top boundary is $Ma_c = 79.6$ (Nield 1964).

Table 2 gives, for different fluid depths, the values of the temperature difference for the appearance of the first pattern ΔT_1, the temperature difference for the appearance of the hexagonal cell pattern ΔT_2, and the corresponding Rayleigh and

No.	d (mm)	ΔT_1 (°C)	ΔT_2 (°C)	R_1	M_1	R_2	M_2
			(100 cs)				
1	2.57	—	5.98	—	—	91.5	76.8
2	1.81	6.68	6.68	35.9	61.0	35.9	61.0
3	1.31	4.12	7.92	8.21	26.4	16.4	52.9
4	0.93	3.86	11.3	2.73	17.5	8.73	56.2
5	0.72	2.09	12.4	0.67	7.17	4.49	48.2
			(50 cs)				
6	1.34	2.88	5.16	13.8	37.0	25.4	68.0
7	0.93	2.74	6.82	4.40	24.5	11.5	63.8

TABLE 2. Temperature difference and non-dimensional numbers of the pattern formation

Marangoni numbers. The lower part of table 2 gives the same parameters for the experiments with the 50 cs oil.

In agreement with our visual observations and with the heat transfer measurements (figure 4) we have set the temperature difference for the onset of the first pattern in the 1.81 mm deep layer equal to the temperature difference for the appearance of the hexagonal pattern. Actually, the first pattern forms, with this fluid depth, just before the hexagonal pattern, but within the experimental error the temperature differences for the formation of both patterns coincide. As can be seen in table 2, the temperature difference at which the first pattern forms decreases systematically with decreased fluid depth, while the temperature difference for the formation of the hexagonal pattern increases with decreased depth. In the 0.72 mm deep layer the Rayleigh number for onset of the first pattern is < 1, the Rayleigh number for onset of the hexagons is only 4.5. The Marangoni number for onset of the first pattern in the 0.72 mm deep layer is only 7, i.e. much smaller than the critical Marangoni number. On the other hand the Marangoni numbers for onset of the hexagonal pattern are near the theoretical critical Marangoni number.

The values of the Rayleigh number as well as the Marangoni number for the onset of both patterns in the 50 cs oil are in each case larger than the corresponding values for the 100 cs oil. The differences are too large to be explained by the experimental uncertainties. There are, on the other hand, not enough data to decide whether or not there is a systematic shift to higher non-dimensional numbers with the 50 cs oil. We emphasize that the visual observations with both oils gave completely analogous results.

We note that the uncertainty in the values of the Rayleigh numbers is of the order of 10 %, because ΔT is known only to about ± 5 %, as discussed before. The depth d is known to about 1 %, so d^3 is known to about 3 %, ν and κ are both known to 1 %. The uncertainty in the values of the Marangoni numbers is also of the order of 10 %. We have measured the value of $\mathrm{d}S/\mathrm{d}T$. The tensiometers used to determine S are accurate to only 1 %. On the other hand, $\mathrm{d}S/\mathrm{d}T$ is quite small, so the error in the determination of $\mathrm{d}S/\mathrm{d}T$ is much larger. We have measured $\mathrm{d}S/\mathrm{d}T$ before (Koschmieder 1967) and found for the 100 cs silicone oil $\mathrm{d}S/\mathrm{d}T = 0.058$ dyne/cm °C. Our present value $\mathrm{d}S/\mathrm{d}T = 0.050$ dyne/cm °C is slightly smaller, but the difference is probably primarily the systematic uncertainty in determining $\mathrm{d}S/\mathrm{d}T$. We do not claim an

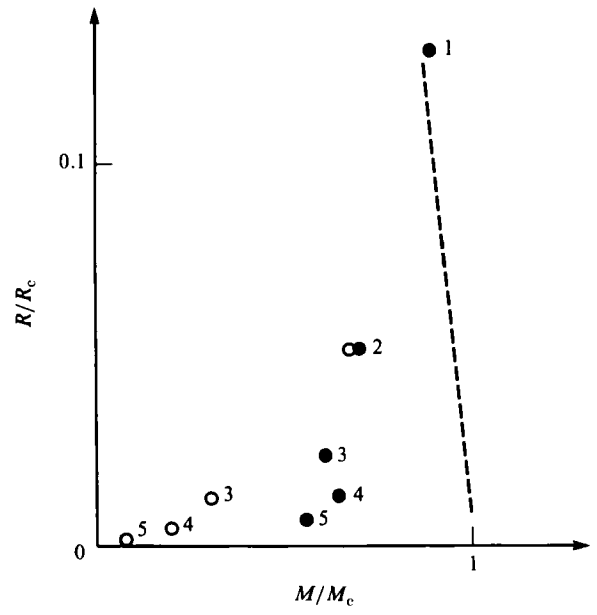

FIGURE 8. Comparison of the normalized Rayleigh and Marangoni number for the onset of convection of the two patterns. Open circles indicate first pattern, full circles indicate hexagonal pattern. The numbers refer to the different layers listed in table 2. The dashed line shows the expected onset of surface-tension-driven convection.

accuracy better than $\pm 5\,\%$. The uncertainty in the Marangoni number is of the order of 10 %, because 5 % comes from $\mathrm{d}S/\mathrm{d}T$, 1 % each from ν and κ and 5 % from ΔT.

For comparison with theory, in particular with figure 1 in Nield (1964), we divide the Rayleigh numbers and Marangoni numbers in table 2 by the corresponding critical numbers. However, the critical values of the numbers for the insulating free surface cannot be used now. The upper thermal boundary condition is taken into account by Nield via the parameter L, which is given here by $L = (\mathrm{d}Nu/\mathrm{d}T)\,\Delta T_{\mathrm{f}}$. The values of $\mathrm{d}Nu/\mathrm{d}T$ follow from figures 4–7. The value of L for the five fluid layers listed in table 2 is $L = 0.19 \pm 0.02$. The critical Marangoni number with $L = 0.19$ is, according to Nield, $M_{\mathrm{c}} = 86.8$, the critical Rayleigh number is then $R_{\mathrm{c}} = 693.5$. Using these critical numbers we arrive at the points shown in figure 8. The dashed line in figure 8 shows the curve for the onset of convection in the presence of buoyancy and surface-tension effects. The critical curve can be written as $R/R_{\mathrm{c}} + M/M_{\mathrm{c}} \approx 1$. As we see in figure 8 the measured points for the onset of the hexagonal pattern are near the critical line. The points deviate from the expected value to lower values of M/M_{c} for the fluid layers with smaller depth. This seems to be a systematic effect. We speculate that this is caused by finite amplitude effects of the flow in the first pattern. Before the formation of the hexagons the motion in the first pattern seems to become so vigorous that the hexagons form prematurely, before one would expect the hexagons to form in a resting fluid layer. The vigorous motion in the first pattern is clearly documented by the increase of the convective heat transfer before the formation of the hexagons (figures 4–7).

The points in figure 8 which mark the onset of the first pattern are clearly subcritical from the point of view of the theory of convection caused by the surface-tension gradient $\mathrm{d}S/\mathrm{d}T$. As the thickness of the fluid layer increases the

difference in the Marangoni number of the onset of the two patterns decreases, until at around 2 mm depth (with this fluid) the hexagonal pattern becomes the only pattern to appear at all. On the other hand, the tendency of the first pattern to appear at ever smaller temperature gradients, or Rayleigh and Marangoni numbers, is quite obvious.

4. Discussion

The principal result of these experiments is the discovery of the unexpected first pattern. In order to observe this pattern it is necessary to work with fluid layers of small depth, in our case smaller than 2 mm. Small depth was involved in Bénard's observation that his cells formed at extraordinarily small Rayleigh numbers and is also a requirement for surface-tension forces to have their full impact.

It has been suggested that there may be three reasons for the theoretically unexpected formation of the first pattern, namely

(*a*) an experimental imperfection;

(*b*) a subcritical instability;

(*c*) an instability not contained in the conventional theories.

An experimental imperfection would be a deviation of the experimental set-up from the case studied in conventional theories, that is from the case of a plane motionless fluid on an infinite horizontal plate heated uniformly from below and cooled uniformly from above through the upper surface which is subject to surface tension effects.

In our apparatus such an imperfection is the meniscus of the fluid layer at the wall, which is not considered in the theories. The meniscus is a natural phenomenon occurring whenever a fluid layer is in a container. In reality the meniscus seems to pose more of a problem than one would expect. We have observed that the silicone oil moves up along the rim as a thin film to a height of over 1 cm if the applied temperature difference is large, probably a consequence of the vertical temperature gradient in the rim. However, the meniscus cannot be the cause of the first pattern because one can arrange a fluid layer without a meniscus and still observe the first pattern. The meniscus was eliminated by containing the fluid with a thin lucite ring (of 102 mm diameter and about 1.4 mm depth). Fluid was put into the bowl formed by the copper bottom plate and the lucite ring so that the level of the fluid was plane with the top of the ring. The first pattern formed as usual.

In connection with the first occurrence of circular cells in our experiments it has been suggested that the first pattern may be caused by lateral heat loss or other radial temperature gradients, such as those caused by the misalignment of the top glass plate or by the non-uniformity of the temperature of the top glass plate caused by the temperature increase of the cooling water. Lateral heat loss in our experiments has practically been eliminated by surrounding the rim of the fluid with vacuum as indicated in figure 1. But this arrangement makes the vertical temperature gradient in the rim smaller than the temperature gradient in the fluid because the cooling at the rim is applied at a greater height above the copper plate than for the glass plate over the fluid layer (figure 1). At the level of the fluid the rim will be warmer than the fluid, i.e. there is a horizontal temperature gradient. However, the lucite rim is a very poor thermal conductor, while the copper on the bottom of the very thin silicone-oil layer is an excellent conductor. Even from the top of the fluid layer the uniform temperature of the copper plate is only about 1 mm away, while the rim is, for a large part of the fluid, some centimetres away. Furthermore, the thermal

conductivity of copper is about 2500 times better than the thermal conductivity of silicone oil. Thus it would require very large temperature differences between the rim and the fluid in order to create an effective horizontal temperature gradient in the interior of the fluid. Also, there is no mechanism known by which small-scale cells would be created via a horizontal temperature gradient in a fluid. Finally the experiment with the fluid contained by a small lucite ring does not support the concept of the significance of the lateral temperature gradient either, because in that set-up the fluid layer is separated from the rim of the apparatus by an air gap of 12 mm width. Air is an excellent thermal insulator which should shield the fluid effectively from the temperature distribution in the rim.

To investigate the non-uniformity of the temperature of the glass lid caused by the increase of the temperature of the cooling water, we measure this temperature increase with the heat sensor. For the extreme case of the lowest fluid depth (0.73 mm) and the largest applied temperature difference across the oil, the temperature increase of the cooling water amounted to 3 % of the temperature difference across the oil. However, the temperature difference in the cooling fluid extends from the centre of the lid to the rim of the lid. If one compares the temperature gradients then the ratio of the temperature gradient across the lid to the vertical temperature gradient across the convecting fluid is about 2×10^{-4}. In order to see whether this has a noticeable effect on the formation of the pattern, we increased the flow rate of the cooling water from the 20 $cm^3\ s^{-1}$ used when we measured with the heat sensor, to the maximal flow rate with this pump which was about 80 $cm^3\ s^{-1}$. The ratio of the radial to the vertical temperature gradient was then 5×10^{-5}. No noticeable consequence of the increased flow rate was observed. We do not, therefore, believe that the radial temperature gradient in the glass lid is significant for the formation of the first pattern.

The misalignment of the plane of the glass lid with respect to the plane of the fluid surface discussed in §3.1 has a potentially greater influence on the uniformity of the top temperature of the fluid, than the non-uniformity of the temperature caused by the cooling. The consequences of the misalignment of the lid on the onset of the hexagonal pattern were obvious in all experiments, see e.g. figure 2(*d*). All efforts to improve on this situation had little or no success. Misalignment of the lid seemed to have little if any effect on the formation of the first pattern, which in all experiments, seemed to form essentially in an axisymmetric and not one-sided way. Figure 2(*a*, *d*) are from the same experiment and show that there is no apparent relation between the symmetry of the formation of the first pattern and the asymmetry of the formation of the hexagonal pattern.

Motion of the air between the fluid and the glass lid might also be the cause for the formation of the first pattern. However, the Rayleigh numbers of the air layer are, even with the highest temperatures applied, smaller than $10^{-3}\ R_c$. The prime reason for this is the very small depth of the air layer (≈ 0.5 mm) and the dependence of the Rayleigh number on the third power of the depth. It seems to be most unlikely that the first pattern is induced by motion of the air layer.

Finally, another possible experimental imperfection might be that the aluminum powder added to the fluid causes the formation of the first pattern. The aluminum powder settles gradually and causes a compensating upward motion of the fluid. However, one would expect any possible effect of the settling of the powder to be smaller in the shallow layers of fluid than in deep layers, because the aluminum powder will settle sooner in the shallow layers and so it seems to be unlikely that the first pattern would appear preferentially in shallow fluid layers. One should also

expect an effect of the concentration of the aluminum particles. The concentration of the particles was varied substantially (we estimate by a factor of at least 10), mainly because of our efforts to take photographs of the flow which requires substantially bigger concentrations of the aluminum powder, but we did not notice any indication that this had influenced the appearance of the first pattern. We know of no theory that would predict the formation of a cellular pattern on the basis of the settling motion of an impurity in a fluid. Such a settling motion is not related to the diffusive two-component Bénard convection problem which has been reviewed by Schechter, Velarde & Platten (1974).

To summarize, we do not see a convincing reason for believing that the first pattern is caused by an imperfection of the experimental set-up.

Concerning the question of the possibility of a subcritical instability we note that a subcritical instability was predicted by Davis (1969). Later, Davis & Homsy (1980) and Castillo & Velarde (1982) elaborated on this topic. Of importance in connection with this problem is the value of the crispation number C, which is a characteristic parameter for the importance of the surface tension coefficient S. C is defined as $C = \mu\kappa/Sd$, where μ is the dynamic viscosity of the fluid. In our experiments the value of C is about 5.5×10^{-4}, so the deformability of the surface is very small. This means that the basic results concerning the subcritical instability are contained in Davis' (1969) paper. From figure 1 therein, it follows for $L = 0$ (we have $L = 0.2$) that the subcritical instability ranges from $Ma = 57$ to $Ma = 80$ at $R = 0$. However, in our experiments with the 0.72 mm deep layer the first pattern appears according to table 2 at $Ma = 7.2$ (with $R = 0.7$), which is deep in the stable region of figure 1 of Davis. So, although according to the energy method a range of instability is predicted which is at a lower Marangoni number than the critical value of the instability predicted by linear theory, the instability apparent in the first pattern that we observe is deep in the stable region according to the energy method. There is also the problem that the subcritical instability is probably associated with the appearance of the hexagonal pattern, and not a pattern of a different form as we observed.

An explanation of the first pattern can be sought in Scriven & Sternling's (1964) paper. The onset of convection driven by surface tension at ever smaller temperature gradients is actually predicted there. There are, however, difficulties. Scriven & Sternling predict that the small onset temperature gradients are accompanied by increased wavelengths or cell sizes. However, we did not observe in any of our experiments a noticeable difference in the size of the cells of the first pattern and the hexagonal pattern. The wavelength of the hexagonal pattern is determined by Nield's theory and does not change with decreased depth of the fluid. It can be seen in figure 2(*d*) that there is no significant difference in the cell sizes of the first pattern and the hexagonal pattern. We did not make a systematic survey of the cell sizes, but we believe that within $\pm 10\%$ accuracy the wavelength of the first pattern and the hexagonal pattern are the same. So there seems to be a discrepancy between the experimental observation and this aspect of Scriven & Sternling's results. Also, it follows from Smith (1966) and Davis & Homsy (1980) that only very small shifts in the critical Marangoni number are expected if the crispation number is as small as it is in our experiments.

Our experimental results for the onset of the hexagonal pattern, are in quite good agreement with the basic results of Pearson (1958) and Nield (1964). Nield's study seems to be particularly relevant because it incorporates gravity, which is present in the laboratory and is of such magnitude that it cannot easily be neglected. The fact that the hexagonal pattern appears in thin layers at subcritical Marangoni

numbers seems to be understandable as a finite-amplitude effect of the first pattern. It appears that Pearson's and Nield's theories correctly predict the consequences of the presence of the surface tension gradient $\mathrm{d}S/\mathrm{d}T$ on convective motions. So the formation of the first pattern, which appears neither in Pearson's nor in Nield's study, is not caused by the variation of surface tension with temperature.

Help and comments from Professor R. S. Schechter and Professor S. H. Davis are gratefully acknowledged. Mr S. Prahl has helped with the visualization experiments. Mr J. Gardner has measured the surface-tension coefficients. Support of this work through the National Aeronautics and Space Agency and through the National Science Foundation is also gratefully acknowledged.

REFERENCES

Bénard, H. 1900 *Rev. Gen. Sci. Pure Appl.* **1**, 1261–1271, 1309–1328.
Bénard, H. 1930 *Proc. 3rd. Int. Congr. Appl. Mech.* **1**, 120.
Block, M. J. 1956 *Nature* **178**, 650–651.
Castillo, J. L. & Velarde, M. G. 1982 *J. Fluid Mech.* **125**, 463–474.
Cloot, A. & Lebon, G. 1984 *J. Fluid Mech.* **145**, 447–469.
Davis, S. H. 1969 *J. Fluid Mech.* **39**, 347–359.
Davis, S. H. & Homsy, G. M. 1980 *J. Fluid Mech.* **98**, 527–553.
Koschmieder, E. L. 1967 *J. Fluid Mech.* **30**, 9–15.
Koschmieder, E. L. 1974 *Adv. Chem. Phys.* **26**, 177–212.
Koschmieder, E. L. & Pallas, S. G. 1974*a* *Intl J. Heat Mass Transfer* **17**, 991–1002.
Koschmieder, E. L. & Pallas, S. G. 1974*b* *Rev. Sci. Instrum.* **45**, 1164–1165.
Kraska, J. R. & Sani, R. L. 1979 *Intl J. Heat Mass Transfer* **22**, 535–546.
Nield, D. A. 1964 *J. Fluid Mech.* **19**, 341–352.
Palmer, H. J. & Berg, J. C. 1971 *J. Fluid Mech.* **97**, 779–787.
Pearson, J. R. 1958 *J. Fluid Mech.* **4**, 489–500.
Rayleigh, Lord 1916 *Phil. Mag.* **32**, 529–546.
Rosenblat, S., Davis, S. H. & Homsy, G. M. 1982*a* *J. Fluid Mech.* **120**, 91–122.
Rosenblat, S., Homsy, G. M. & Davis, S. H. 1982*b* *J. Fluid Mech.* **120**, 123–138.
Scanlon, J. W. & Segel, L. A. 1967 *J. Fluid Mech.* **30**, 149–162.
Schechter, R. S., Velarde, M. G. & Platten, J. K. 1974 *Adv. Chem. Phys.* **26**, 265–301.
Schmidt, R. J. & Milverton, S. W. 1935 *Proc. R. Soc.* A **152**, 586–594.
Scriven, L. E. & Sternling, C. V. 1964 *J. Fluid Mech.* **19**, 321–340.
Silveston, P. L. 1958 *Forsch. Ing. Wes.* **24**, 29–32, 59–69.
Smith, K. A. 1966 *J. Fluid Mech.* **24**, 401–414.